Rigid Amorphous Fraction in Isotactic Polypropylene

Qamer Zia, Daniela Mileva, and René Androsch*

Center of Engineering Sciences, Martin-Luther-University Halle-Wittenberg, D-06099 Halle/S., Germany

Received June 30, 2008; Revised Manuscript Received August 15, 2008

ABSTRACT: The rigid amorphous fraction in isotactic polypropylene is comprehensively analyzed as a function of the history of crystallization. The crystallinity, crystal morphology, and superstructure were independently and precisely controlled by the rate of cooling on melt crystallization and by the temperature/time of subsequent annealing. Formation of lamellae and spherulites on slow cooling and formation of nodular domains on rapid cooling are observed. Annealing allowed an increase of the crystallinity and perfection/growth of crystals, without affecting their habit and higher order organization. Analysis of the glass transition of the amorphous phase in preparations with a crystallinity between 40% and 75% proves coexistence of differently mobile amorphous structures. The rigid amorphous fraction and the ratio between rigid and mobile amorphous fractions decrease with increasing crystallinity, which is due to reduced covalent coupling of crystals and amorphous phase in preparations of high crystallinity. Analysis of the effect of the crystal habit on the rigid amorphous fraction allows identification of the structure at the basal planes of crystals as a major source of the immobilization of the amorphous phase. The mobile amorphous fraction cannot primarily be related to interspherulitic or interlamellar stack regions of the semicrystalline superstructure. The presence of crystals in semicrystalline isotactic polypropylene also affects the properties of the mobile amorphous fraction, which is detected by a distinct decrease of its glass transition temperature in samples of high crystallinity, which contain crystals of high stability. This confirms increasing decoupling of the crystalline and amorphous phases in preparations of high crystallinity, as was independently derived by the analysis of the rigid amorphous fraction.

1. Introduction

Semicrystalline polymers consist of a crystalline and an amorphous phase. These phases are coupled at the interface by covalent bonds since the macromolecules usually traverse between them.[1,2] As a consequence, the properties of such coexisting, at the interface interconnected crystalline and amorphous phases, are different from those of isolated crystals and the bulk liquid/glass. This includes in particular the mobility of molecule segments in the amorphous phase.[3] The covalent linkage of the crystalline and amorphous phases at the crystal surfaces results in a decrease of the number of microconformations, which can be adopted by amorphous molecule segments in crystal-near regions, if the particular macromolecule is part of both the crystalline and amorphous phases. This is caused by the locked microconformation of molecule segments when entering the crystalline register. The dimensions of the crystalline−amorphous transition layer and the magnitude of the immobilization of the amorphous phase probably are controlled by the chain architecture, i.e., by the inherent flexibility of the macromolecule, and by the structure of the crystal surfaces, which is adjustable within limits by the condition of crystallization. The present study is an attempt to quantify the immobilization of the amorphous phase in semicrystalline isotactic polypropylene (iPP) of different histories of crystallization to derive conclusions about the effect of the crystalline−amorphous superstructure, including crystallinity, and higher order organization of the crystals.

The loss of segmental mobility of parts of the amorphous phase due to coupling to crystals causes a decrease of the specific heat capacity and an increase of the glass transition temperature. Therefore, it can quantitatively be assessed by thermal analysis.[3] Early evidence for hindrance of segmental mobility of amorphous chain segments due to the presence of crystals was collected by analysis of the dielectric behavior in aromatic polyesters, although a fractionation of the amorphous phase was not suggested.[4] The existence of differently mobile amorphous fractions was then proposed in a study about the morphology and the modulus of elasticity of semicrystalline poly(ethylene terephthalate) of different crystallinities.[5] Shortly after, it was shown that the intensity of the glass transition in semicrystalline polycarbonate can best be explained "as a linear combination of intensities from the bulk amorphous regions and from non-crystalline polymer within semicrystalline aggregates such as spherulites".[6] At this time, the term *rigid amorphous fraction* (RAF) has been introduced for denotation of the less mobile amorphous structure.[7] Note that the term *rigid amorphous*, in this context, is not related to the actual state of vitrification, but rather points to the existence of a restraint amorphous structure with an increased glass transition temperature. Formation of an RAF is nowadays evidenced for almost all semicrystalline polymers, including polyethylene,[8,9] isotactic and syndiotactic polypropylene,[10,11] isotactic poly-1-butene (iPB-1),[12] polyamide 6 (PA 6),[13] poly(ethylene terephthalate) (PET),[14,15] poly(butylene terephthalate) (PBT),[16,17] polycarbonate (PC),[6,11,18] or poly(hydroxybutyrate) (PHB).[11] An up-to-date list of polymers which show formation of an RAF is published elsewhere.[19]

Present research activities exceed the plain proof of existence of differently mobile amorphous fractions in semicrystalline polymers. Recently, an immobilization of the amorphous structure has also been confirmed in noncrystallizable poly(methyl methacrylate) (PMMA) in the presence of silica nanoparticles[20] and in semicrystalline hydroxybutyrate oligomers, which form extended chain crystals.[21] Both studies suggest that covalent bonding between the amorphous phase and immobilizing impurity may not implicitly be required. Moreover, the investigation of the silica-filled PMMA allowed conclusions to be drawn about the temperature of vitrification/devitrification of the RAF. The data showed that the origin/source for restriction of the mobility of parts of the amorphous phase must appear/disappear before the RAF does vitrify/

* To whom correspondence should be addressed. Phone: +49 3461 46 3762. Fax: +49 3461 46 3891. E-mail: rene.androsch@iw.uni-halle.de.

10.1021/ma801455m CCC: $40.75
Published on Web 10/07/2008

devitrify. Generalization of this conclusion implies that crystals in semicrystalline polymers must melt before the RAF can relax. Analysis of the evolution of the specific heat capacity on isothermal melt crystallization of PC or PHB supports this result.[11] Investigation of the glass transition temperature of the RAF of iPB-1, in contrast, showed that devitrification of the RAF on heating occurs gradually in a wide temperature range of more than 50 K. More importantly, the study showed that devitrification of the RAF was completed at a temperature well below the melting temperature of crystals.[12] These, apparently contradictory, exemplary results reveal that a representative rule regarding the temperature of vitrification/devitrification of the RAF probably does not exist.

Further, recently intensified research activities include the in-depth analysis of the exact location of mobile and rigid amorphous fractions in the semicrystalline superstructure and the establishment of quantitative correlations between the RAF and the condition of crystallization. Despite the ongoing debate of whether the mobile amorphous fraction (MAF) is located within stacks of lamellae,[13,22] there seems to be consensus about the location of the RAF at the crystal basal planes. Qualitative and quantitative information about the effect of the fine structure of the crystal basal planes, including, e.g., the number of molecules which traverse the crystal−amorphous interface, on the RAF and its properties does not exist. We follow the idea that a variation of the condition of crystallization affects the crystal morphology including the fine structure at the crystal basal planes and the covalent link with the amorphous phase. Comparison of the phase structures of melt-crystallized and initially quenched and subsequently cold-crystallized PET showed an about 50−100% larger RAF of the latter preparation, despite identical crystallinities.[23] Similarly, a low temperature of crystallization, or crystallization at a high cooling rate, revealed a larger RAF in the case of iPB-1.[12] These data point to larger molecular coupling between crystalline and amorphous phases in the case of small and imperfect crystals with irregular folding of molecules at the basal planes. Annealing of such imperfect crystals at elevated temperature resulted in a decrease of the RAF, probably due to perfection of the fold surface of the crystals.[24,25] Thus, it can be concluded that for a given polymer the RAF is adjustable and, with that, ultimate properties,[12,23−26] despite a variation of the RAF, independent of the semicrystalline superstructure may not be possible.

As far as we are aware, a direct correlation between the RAF and number and morphology of crystals, based on a systematic investigation, has not yet been established for iPP. Formation of an RAF in iPP is directly evidenced by a few studies only, employing calorimetry and nuclear magnetic resonance (NMR) techniques.[27,28] These studies suggest a considerable amount of rigid amorphous structure of 25−30%, [27] or close to 40%,[28] in semicrystalline iPP at ambient temperature. Due to the different thermal history and molecular structure of the specific specimen, these data, naturally, cannot directly be compared; however, they point to the importance of consideration of the RAF for a correct and complete description of the structure of iPP. This in particular is true since the existence of differently mobile amorphous fractions in iPP may be related to physical aging. Analysis of the structure of quenched samples as a function of time showed constancy of the crystallinity, but densification of the amorphous structure, accompanied by formation of a constrained, rigid amorphous part and additional reduction of the mobility of the remaining mobile amorphous fraction.[29]

The immobilization of the amorphous phase in semicrystalline iPP is furthermore indirectly indicated by observation of a distinct increase of the glass transition temperature of the mobile amorphous fraction, as is documented in numerous studies. Reports about the glass transition temperature of completely amorphous iPP suggest values between 243 and 258 K.[30−34] Analysis of the glass transition temperature of completely amorphous polypropylene employed both noncrystallizable, atactic polypropylene (aPP) and crystallizable iPP. In the case of iPP, it was found that the cooling rate on primary melt crystallization must exceed $(0.6-1) \times 10^3$ K s^{-1}; otherwise the crystallization cannot be inhibited.[35,36] Furthermore, quenching needed to be performed to temperatures lower than the glass transition temperature. Heating of fully amorphous iPP to temperatures above the glass transition immediately triggered recrystallization of the strongly supercooled liquid by formation of small mesomorphic domains. Simultaneously, the glass transition temperature increases by 20−40 K to about 275−290 K;[30,33] i.e., the presence of small heterogeneities resulted in a major change of the properties of even the mobile amorphous fraction. Unfortunately, the analysis of the RAF was not part of these studies.

Summarizing the scope of the present work, we intend to systematically and quantitatively investigate the effect of the semicrystalline superstructure on the formation of an RAF in iPP. To achieve this goal, specimens of largely different crystal morphologies and crystallinities were prepared by variation of the rate of cooling on primary melt crystallization and subsequent annealing. As a result of the specific history of crystallization, we were able to generate specimens of identical crystallinities, which contain crystals of qualitatively different morphologies/habits. With the analysis of the RAF of such samples, we attempt to gain further insight/knowledge about critical structural features and about the mechanisms of formation of the RAF in semicrystalline polymers.

2. Experimental Section

2.1. Materials. We used an iPP from Montell Polyolefins with a mass-average molar mass and a polydispersity of 373 kg mol^{-1} and 6.2, respectively. Films of 100 μm thickness were prepared from as-received pellets by compression-molding. Subsequently, in a second preparation step, these films were nonisothermally melt-crystallized at rates of cooling between 10^{-1} and 10^3 K s^{-1}, using a special device for controlled rapid cooling, as described elsewhere.[37] The variation of the rate of cooling on primary melt crystallization allowed preparation of semicrystalline iPP with mesomorphic nodules or monoclinic lamellae of different sizes. It is important to note that the temperature of the coolant, i.e., cold water, was 279 K, which is a temperature higher than the glass transition temperature of the amorphous phase. Therefore, none of the samples were crystallized from the glassy state. Before structural analyses, the samples were equilibrated by long-term storage at ambient temperature. This allowed completion of physical aging of the amorphous phase[29] and continuation of crystallization of samples which initially were nonisothermally crystallized at a rate of about 10^2 K s^{-1} or faster. [35] Further modification of the initial structure was achieved by annealing at elevated temperature for a period of 60 min, using a Leitz microscope hot stage 1350 in combination with a Rheometric Scientific temperature controller. The programmed rate of temperature change for approaching the isothermal annealing temperature and for subsequent cooling to ambient temperature was 20 K min^{-1}. Details about the phase structure and the structure and morphology of the crystals are published elsewhere.[38−41]

2.2. Instrumentation. Atomic force microscopy (AFM) was used for direct analysis of the morphology of the crystals. We used a Quesant Universal SPM, which was equipped with a 5 μm × 5 μm scanner. Phase-mode images were collected at ambient temperature using a silicon cantilever NSC 14 with a resonant frequency and force constant of about 170 kHz and 5 N m^{-1}, respectively. The presence or absence of spherulitic superstructure was proven using a DMRX polarizing optical microscope from Leica.

Dynamic mechanical analysis (DMA) was used for measurement of the glass transition temperature of iPP of different histories of

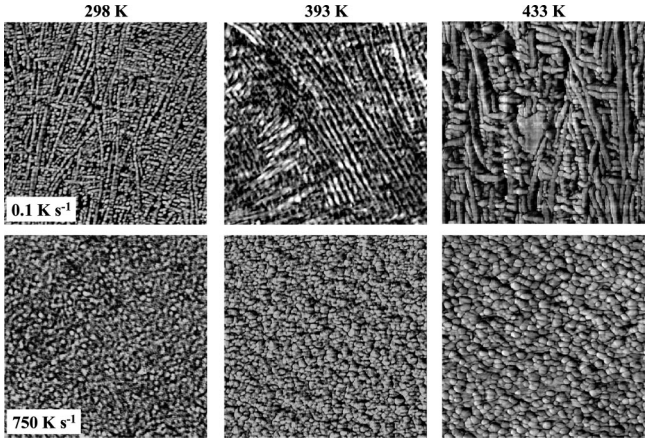

Figure 1. AFM phase-mode images of iPP of different histories of crystallization. The top and bottom rows show the structure of samples which initially were melt-crystallized at 0.1 and 750 K s^{-1}, respectively, before annealing (left) and after annealing for a period of 60 min at 393 K (center) and 433 K (right). The images represent an area of 1 μm × 1 μm.

crystallization. Data were collected in threshold-tensile mode using the Mk III system from Rheometric Scientific. The cross-section and the gauge length of the samples were 0.1 × 5 mm^2 and 8 mm, respectively. The samples were subjected to sinusoidally oscillating strain with a maximum programmed amplitude of 0.1% and a constant frequency of 1 Hz. The samples were cooled to a minimum temperature of 223 K, thermally equilibrated for a period of 5 min, and then heated at a constant rate of 2 K min^{-1}. Glass transition temperatures were observed by the maximum of the loss factor.

Differential scanning calorimetry (DSC) was employed for analysis of the glass transition temperature of the mobile amorphous structure and for evaluation of the crystalline, mobile, and rigid amorphous fractions of the samples of different histories of crystallization. We used a DSC 7 from Perkin-Elmer, in combination with the cryogenic cooling accessory CCA 7. The heat sink temperature was adjusted to 203 K. The sample and reference furnaces were purged with nitrogen at a flow rate of 35 mL min^{-1}. The temperature and heat flow rate were calibrated using metal standards, as described in textbooks.[42] Heat flow rate raw data were collected on heating at a rate of 40 K min^{-1}. The sample mass was 5−10 mg, which was achieved by stacking of several layers of the thin films. We used 20 μL aluminum pans from Mettler-Toledo for encapsulation, with the difference of the mass of the sample and reference pans being less than 0.2%. Heat flow rate raw data were converted to apparent specific heat capacity data after subtraction of a baseline, recorded at identical experimental conditions, in the absence of a sample. Sapphire was used for final calibration of heat capacity data. Glass transition temperatures of the mobile amorphous fraction were determined as the half-devitrification temperature on heating.[42] The calculations of the enthalpy-based crystallinity as a function of temperature and of the rigid amorphous fraction at the temperature of the glass transition of the mobile amorphous structure are described in detail elsewhere.[3,43] Data of the heat capacity and of the enthalpy of liquid and solid iPP, which are needed for the calculations, were taken from the ATHAS database.[44]

3. Results and Initial Discussion

3.1. Crystal Morphology and Spherulitic Superstructure. Figure 1 shows AFM phase-mode images of iPP of different histories of crystallization representing an area of 1 μm × 1 μm. The images were selected from a larger set of micrographs for demonstration of the effect of variation of (a) the rate of cooling on melt-crystallization and (b) the conditions of subsequent annealing on the supermolecular, semicrystalline structure of iPP. The top row shows images taken on samples which initially were melt-crystallized at a rate of cooling of 0.1 K s^{-1} before annealing (left) and after annealing at 393 K (center) and 433 K (right). The micrographs reveal formation of cross-hatched lamellae with an initial thickness of about 10−15 nm. The thickness of the lamellae increases on annealing as a function of temperature and time,[45−47] reaching a maximum value of about 25−30 nm. The images of the bottom row were obtained on samples which primarily were crystallized on fast cooling at a rate of 750 K s^{-1} and subsequent annealing at ambient temperature. Monoclinic lamellae are replaced by mesomorphic nodules with a size of less than 20 nm, being in accord with numerous studies about the structure of quenched iPP.[30−34,48,49] The transition from formation of monoclinic lamellae to formation of mesomorphic nodules occurs at a critical cooling rate of about 10^2 K s^{-1}.[37,39,50] Heating of nodules triggers a phase transition from the mesomorphic structure to a monoclinic structure[51−53] and an increase of the size to about 40−50 nm. In the context of the present study, it is important to recognize that the shape of nodular crystals nearly does not change on annealing.

Polarizing optical microscopy reveals formation of a space-filling spherulitic superstructure in samples which were melt-crystallized at rates lower than about 10^2 K s^{-1}. Melt crystallization at higher rates completely suppresses the formation of spherulites. It is important to note that subsequent annealing, regardless of the temperature and time, does not affect the presence or absence of spherulites.

The exemplary images of Figure 1 illustrate that a large variety of qualitatively and quantitatively different semicrystalline structures can be generated by controlling the rate of cooling on melt crystallization and the time and temperature of subsequent annealing. Selection of the cooling rate on melt crystallization predetermines the shape of the crystals, since it controls whether lamellae or nodules are formed. The choice of the conditions of subsequent annealing permits a precise adjustment of the size and the thermodynamic stability of the crystals, without affecting the external habit of the crystals and their organization in higher order structures. A complete overview of the structures, including the pathway of generation, is given elsewhere.[39,41]

3.2. Enthalpy-Based Crystallinity. Figure 2 shows estimates of the enthalpy-based crystallinity of iPP at room temperature as a function of the rate of cooling during primary melt crystallization. The crystallinity data were calculated from temperature-dependent apparent specific heat capacity data. Reference values of the specific heat capacity of liquid and solid iPP and of the specific enthalpy of fusion were taken from the ATHAS database. [44] We are aware that the listed, bulk specific enthalpy of fusion of iPP holds for monoclinic crystals only. Therefore, we need to acknowledge some uncertainty in the calculation of the crystallinity of samples which contain non-monoclinic, mesomorphic crystals/domains. We assume that the error is rather small since the specific enthalpies of fusion of mesomorphic and monoclinic structures differ by less than 15−20%[54] and, more important, since the phase transition from mesomorphic to monoclinic structure occurs well below about 370 K. The majority of crystals, however, melt above this temperature.

The filled and open squares in Figure 2 represent data collected from samples which contain monoclinic lamellae or mesomorphic nodules. The crystallinity decreases, as expected, with increasing cooling rate on melt crystallization due to increasing kinetic restriction of the diffusion-controlled crystallization process. We obtained an enthalpy-based crystallinity of close to 60% for iPP, which is slowly cooled at a rate of 0.1 K s^{-1}. The microstructure of this particular preparation is shown in Figure 1 with the top left image. The crystallinity decreases

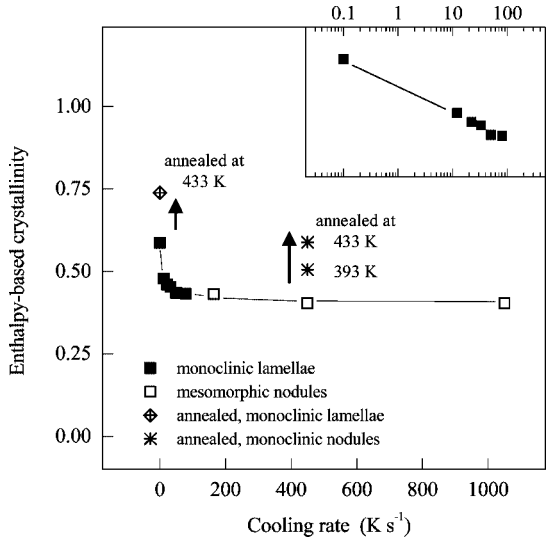

Figure 2. Enthalpy-based crystallinity of iPP as a function of the rate of cooling on initial melt crystallization. The filled and open squares represent data which were obtained on non-annealed samples containing lamellae or nodules, respectively. The effect of annealing on the crystallinity is illustrated for selected samples with the cross-filled tilted square and asterisks. The inset is a plot of the crystallinity of samples with monoclinic lamellae (filled squares) as a function of the logarithm of the cooling rate.

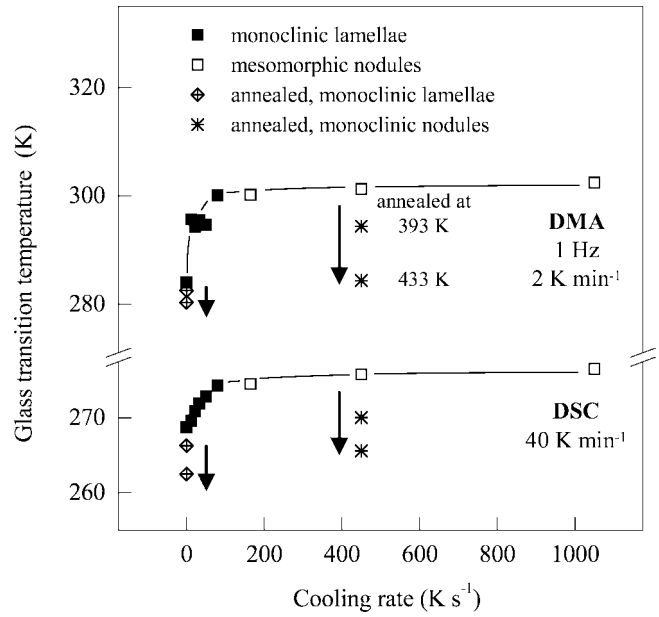

Figure 3. Glass transition temperature of iPP as a function of the rate of cooling on initial melt crystallization. The filled and open squares represent data which were obtained on non-annealed samples containing lamellae or nodules, respectively. The effect of annealing on the crystallinity is illustrated for selected samples with the arrows and the cross-filled tilted squares and asterisks. Data were obtained using DMA (upper set of data points) and DSC (lower set of data points).

to about 40% on increasing the cooling rate to about 10^2 K s^{-1}. The decrease of the crystallinity can be described by an exponential law, which is demonstrated with the inset in Figure 2, where data are plotted as a function of the logarithm of the cooling rate. This, however, only is true for samples which were crystallized at a rate lower than 10^2 K s^{-1}, since annealing of such samples at ambient temperature does not increase the crystallinity. A further increase of the cooling rate is connected with changes of (a) the crystal structure from monoclinic to mesomorphic, (b) the crystal habit from lamellae to nodules, and (c) the superstructure from spherulitic to non-spherulitic. The enthalpy-based crystallinity remains at a constant value of about 40% and is independent of the rate of cooling between 10^2 and 10^3 K s^{-1}, since annealing at room temperature allows completion of crystallization. The microstructure of such a sample is presented in Figure 1 with the bottom left image. The independence of the crystallinity on the cooling rate between 10^2 and 10^3 K s^{-1} is paralleled by the observation of identical crystal morphologies, i.e., identical sizes and habits of the nodules. Annealing at elevated temperature results in an increase of the crystallinity, which, for selected samples, is illustrated in Figure 2 with the cross-filled tilted square and asterisks. The crystallinity of iPP, which initially was crystallized on slow cooling at 0.1 K s^{-1}, increases from 60% to 70−75% by annealing at 433 K for a period of 60 min (cross-filled tilted square). The corresponding AFM structure is shown with the top right image in Figure 1. Annealing of a nodular preparation (open squares) leads to a maximum increase of the crystallinity from initially 40% to about 60% (asterisks). Simultaneously, the crystal structure changes from mesomorphic to monoclinic. The nodular shape of the crystals is preserved during annealing, as is evidenced with the center and right bottom images in Figure 1.

3.3. Glass Transition Temperature. Figure 3 shows the glass transition temperature of the mobile amorphous fraction of iPP as a function of the rate of cooling on melt-crystallization. Measurements were performed by DMA (upper set of data-points), and by calorimetry (lower set of data-points). The DMA data, consistently, are about 20−25 K higher than the DSC data, which is attributed to largely different frequency of perturbation during measurement.[55,56] The filled and open squares represent data obtained on non-annealed samples, containing monoclinic lamellae and mesomorphic nodules, respectively. The glass transition temperature of iPP, which was melt-crystallized at a rate of 0.1 K s^{-1}, shows a DMA glass transition temperature of about 282 K. An increase of the cooling rate on melt-crystallization to 10^2 K s^{-1} leads to an increase of the glass transition temperature to about 300 K. A further increase of the cooling rate to 10^3 K s^{-1} is not connected with a major change of glass transition temperature, despite the crystal shape changes from lamellae to nodules. This observation is paralleled by independence of the enthalpy-based crystallinity on the rate of cooling between 10^2 and 10^3 K s^{-1}. Annealing at elevated temperature results in a decrease of the glass transition temperature, as is indicated with the downward arrows in Figure 3. The reduction of the glass transition temperature is more distinct for samples of low crystallinity (asterisks), and less pronounced for preparations of initially high crystallinity (cross-filled tilted squares). The data suggest that the decrease of the glass transition temperature by annealing is proportional to the simultaneous increase of the crystallinity.

Figure 4 shows the correlation between the glass transition temperature of iPP of different histories of crystallization and the enthalpy-based crystallinity, with the raw data shown already in Figures 2 and 3. The meaning of the symbols is identical to that of Figures 2 and 3. The glass transition temperature of the mobile amorphous fraction decreases non-linearly with increasing crystallinity within the range of available samples. Most striking, regardless of the exact pathway of crystallization and the shape of the crystals, the data fit a single function. In other words, apparently, it does not matter whether a crystallinity of about 60% was achieved by slow melt crystallization at a rate of 0.1 K s^{-1} or by fast cooling at a rate of 450 K s^{-1} and subsequent annealing at 433 K. The glass transition temperatures, in both cases, are almost identical, as indicated in Figure 4 by the gray-shaded, framed rectangle.

3.4. Rigid Amorphous Fraction. Figure 5a shows the RAF of iPP of different histories of crystallization as a function of

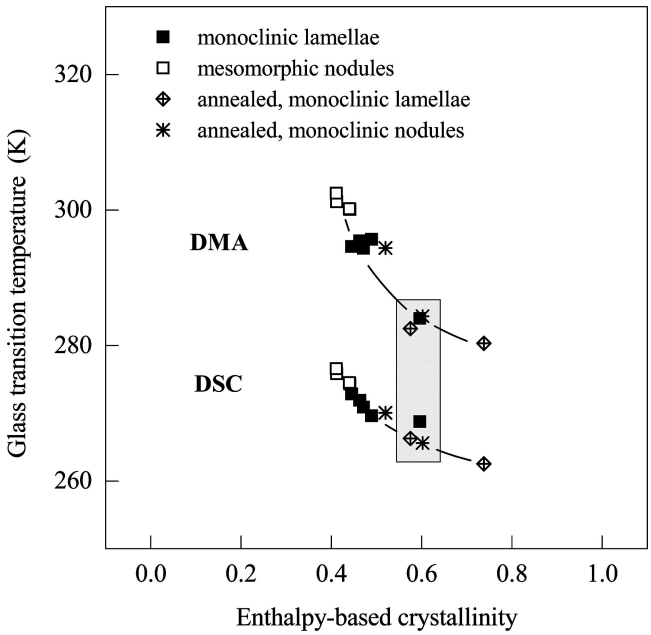

Figure 4. Glass transition temperature of iPP as a function of the enthalpy-based crystallinity. The filled and open squares represent data which were obtained on non-annealed samples containing lamellae or nodules, respectively, and the cross-filled tilted squares and asterisks represent data which were obtained on annealed samples. Data were measured using DMA (upper set of data points) and DSC (lower set of data points).

the enthalpy-based crystallinity, with the meaning of the symbols identical to that in the previous figures. The diagonal indicates the total amorphous fraction (= 1 − crystallinity). The two vertical arrows, labeled RAF and MAF, illustrate an option of easy reading of data in terms of fractions. The experimental data indicate that the absolute RAF decreases with increasing crystallinity, regardless of the specific history of crystallization, habit of crystals, or presence/absence of higher order structures. For example, the RAF of iPP which was prepared by slow cooling at 0.1 K s^{-1} is identical to the RAF in iPP which initially was quenched at a rate of 450 K s^{-1} and subsequently annealed at 433 K for a period of 60 min. The shapes of the crystals in these specific preparations are largely different since the slowly cooled sample contains lamellae and the initially quenched sample contains nodules. The data points which correspond to these preparations are circled in Figure 5a for easy identification. We added an additional data point at zero crystallinity in Figure 5a since we assume that the RAF is absent in completely amorphous samples. This assumption implies that the dependence of the RAF on the enthalpy-based crystallinity passes a maximum, which, however, falls into the region between 0 and about 40% crystallinity, not accessed in the present study.

Figure 5b shows the relative ratio between the RAF and MAF of iPP of different histories of crystallization as a function of the enthalpy-based crystallinity. It decreases within the investigated range of crystallinities between 40% and 75%. The ratio RAF/MAF is almost 2 in iPP of 40% crystallinity; i.e., the RAF is 2 times the MAF. The ratio decreases in iPP of high crystallinities to about unity; i.e., the RAF and MAF are about identical. These data indicate that an increase of the crystallinity between 40% and 75%, at least in the particular case of iPP, is connected to an increase of the average mobility of the amorphous phase, pointing to a reduction of the coupling between amorphous and crystalline phases.

4. Final Discussion and Conclusions

The present study is an attempt to further analyze the reduction of the mobility of molecule segments in the amorphous

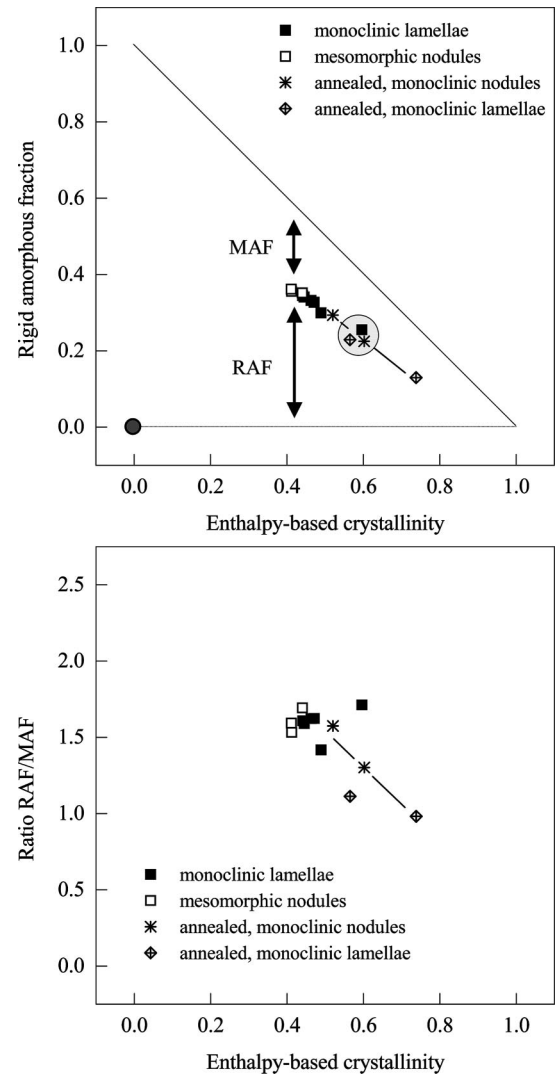

Figure 5. (a, top) RAF of iPP of different histories of crystallization as a function of the enthalpy-based crystallinity. The filled and open squares represent data which were obtained on non-annealed samples containing lamellae or nodules, respectively, and the cross-filled tilted squares and asterisks represent data which were obtained on annealed samples. The diagonal shows the total amorphous fraction. (b, bottom) Ratio between the RAF and MAF of iPP of different histories of crystallization as a function of the enthalpy-based crystallinity. The filled and open squares represent data which were obtained on non-annealed samples containing lamellae or nodules, respectively, and the cross-filled tilted squares and asterisks represent data which were obtained on annealed samples.

phase due to the presence of crystals in semicrystalline polymers. Qualitative evidence about an immobilizing effect of crystals on the amorphous phase was collected for numerous polymers.[19] In contrast, only a few studies focused on detailed and systematic investigation of the effects of the crystallinity, crystal morphology, and superstructure on the immobilization of the amorphous phase. These include in particular PET since in this case a wide range of semicrystalline superstructures can be generated by variation of the condition of crystallization.[15,23−25] Similar research, i.e., investigation of the RAF as a function of the crystallinity, crystal morphology, and higher order superstructure, has not yet been performed on iPP, despite the fact that formation of an RAF has been confirmed in the literature.[19,27−29] The data of the present research, qualitatively and quantitatively, support the results of earlier reports about the formation of an RAF in iPP. As an example, we observed an RAF of about 30−35% in samples with a crystallinity of 40−50% (filled squares in Figure 5a), which compares with an RAF of 26%

obtained in a specific Ziegler−Natta-type iPP of 50% crystallinity, reported in the literature.[27]

The advance of the present study is the availability and investigation of a large set of samples of iPP of identical chemistries but different physical superstructures, generated by variation of the condition/pathway of crystallization. The most important conclusions from the experimental data of this study include proof (I) that the amount of immobilized amorphous structure, relative to the total amorphous fraction, decreases with increasing crystallinity if the crystalline fraction exceeds 40% (Figure 5b), (II) that the RAF, in samples of identical crystallinities, is not largely affected by the lateral size of the crystals, and (III) that there exists a distinct correlation between the mobility of the MAF and the amount of RAF, pointing to coupling of the RAF and MAF. These issues will be explained in more detail in the following paragraphs.

4.1. Effect of Crystallinity on the RAF. The fraction of crystals present in semicrystalline preparations controls the total amount of the RAF. For samples of low crystallinity, it is expected that the RAF increases linearly with increasing total surface area of the basal planes of the crystals, i.e., with increasing crystallinity in the case of predominant lateral crystal growth in the stage of primary crystallization. We suggest that the incremental increase of the RAF per increase of crystallinity (= Δ(RAF)/Δ(crystallinity)) in the stage of primary crystallization is affected by (a) the inherent flexibility of a macromolecule of specific chemistry, being controlled by the number of possible microconformations and the energy barriers between them, and (b) the conditions of crystallization, which controls, within limits, the crystal surface structure/coupling of crystalline and amorphous phases. The range of crystallinity in which a linear increase of the total RAF can be observed was not accessed with the preparations of the present study, and is therefore sketched in Figure 6a. It is an extension of Figure 5a and shows experimental RAF data of iPP (filled squares) and PET (open squares)[25] as a function of the crystallinity. The diagonal represents the total amorphous fraction (RAF + MAF), and the newly inserted lines, labeled 1 and 2, which start at the origin, illustrate the increase of the total RAF in the range of incompleted primary crystallization. The data, obtained in a previous study on cold-crystallized PET (open squares, line 1), suggest a slope Δ(RAF)/Δ(crystallinity) of about 2−3 (∼0.4/0.15); i.e., the increase of the RAF is about 2−3 times the increase of the crystallinity. For iPP of the present study, only a lower limit of Δ(RAF)/Δ(crystallinity) of about unity (∼0.35/0.40) can be estimated from the experimental data (filled squares, line 2).

The initial increase of the RAF within increasing crystallinity, for the polymers analyzed, stops before complete immobilization of the entire amorphous phase. In other words, in both cases, iPP and PET, there is left a mobile amorphous fraction in all samples of different crystallinities, which can directly be deduced from the difference between RAF data points and the diagonal in Figure 6a. The exact reason for this observation is difficult to trace and can be manifold. Initially, the MAF was related to amorphous structure in interspherulitic regions, since it was assumed that the amorphous phase within spherulites may completely be immobilized, or exhibits, at least, a reduced relaxation strength.[6,7,15] Later analyses of semicrystalline space-filled spherulitic systems, using small-angle X-ray scattering and dielectric spectroscopy, led to an assignment of the MAF to amorphous regions between stacks of lamellae.[22,57] Recently, on the basis of research on PA 6, close proximity of the MAF and RAF was suggested; i.e., MAF and RAF are proposed to exist within stacks of lamellae.[13] Regardless of the diversity of observations regarding the exact localization of RAF and MAF, full immobilization of the amorphous phase does not seem to

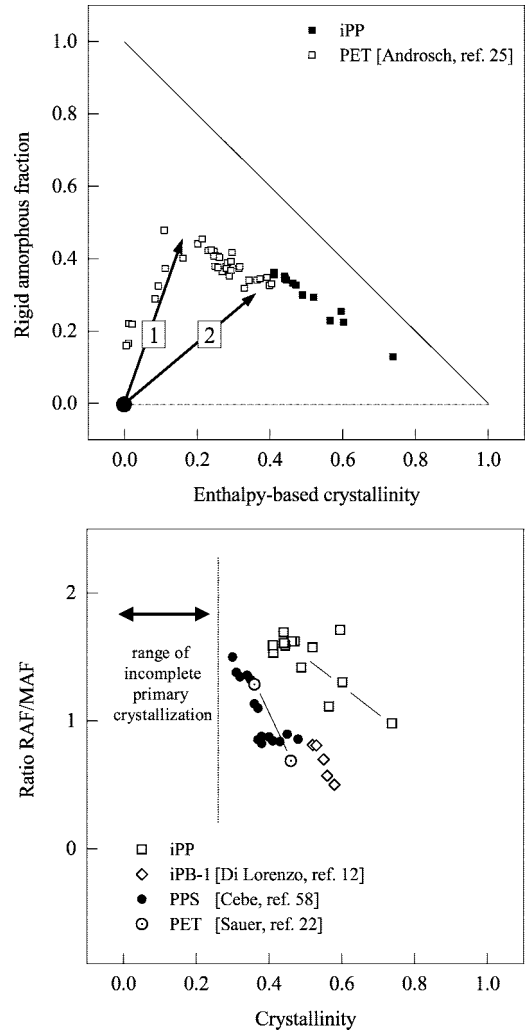

Figure 6. (a, top) RAF of iPP (filled squares) and PET (open squares)[25] as a function of the enthalpy-based crystallinity. The diagonal represents the total amorphous fraction. The lines, labeled 1 and 2, indicate the expected increase of the RAF with increasing crystallinity for two polymers with different tendencies for formation of an RAF. (b, bottom) Ratio between the RAF and MAF of iPP, iPB-1,[12] PPS,[58] and PET[22] as a function of the crystallinity.

be typical in semicrystalline polymers, independent of the crystallinity (see, e.g., Figures 5a and 6a), independent of spherulitic or nonspherulitic crystallization, and independent of the existence of stacks of lamellae or nonlamellar crystals. Note that preparations with nodules (Figure 1, bottom row) are of nonspherulitic superstructure and preparations with lamellae (Figure 1, top row) are of space-filled spherulitic superstructure.[39,50] We conclude therefore that formation of RAF, at least for the iPP of the present work, occurs at a very local scale in close proximity of crystals only and that the MAF must not necessarily be related to nonspherulitic regions or amorphous structure outside the lamellar stacks.

In addition to the detection of preservation of a mobile amorphous fraction, we even observed that the ratio between the RAF and MAF decreases with increasing crystallinity (Figure 5b). Reinspection of selected RAF data, available in the literature, and recalculation of the ratio RAF/MAF confirms our observation that the immobilization of the amorphous phase is reduced in samples of relatively high crystallinity. Figure 6b shows the ratio RAF/MAF as a function of crystallinity for the iPP of the present study, PET,[25] iPB-1,[12] and poly(phenylene sulfide) (PPS).[58] The ratio RAF/MAF decreases in all of these examples. Note that the selection of examples, shown in Figure

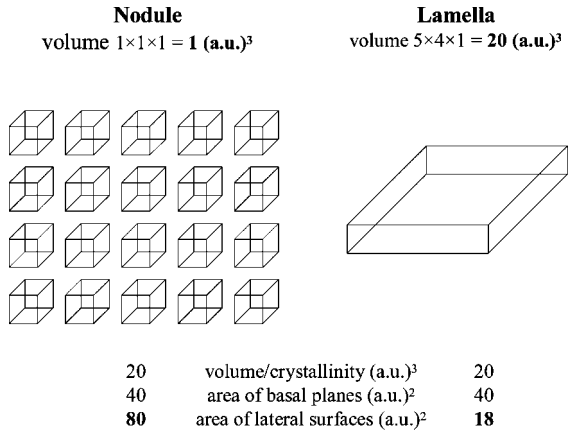

Figure 7. Schematic of nodules (left) and a lamella (right). The length of the edges is selected such that the volume and the area of the basal planes of 20 nodules are identical to those of a single lamella. The total area of the lateral surfaces of the nodules, in contrast, is about 4× the total area of the lateral surfaces of the lamella.

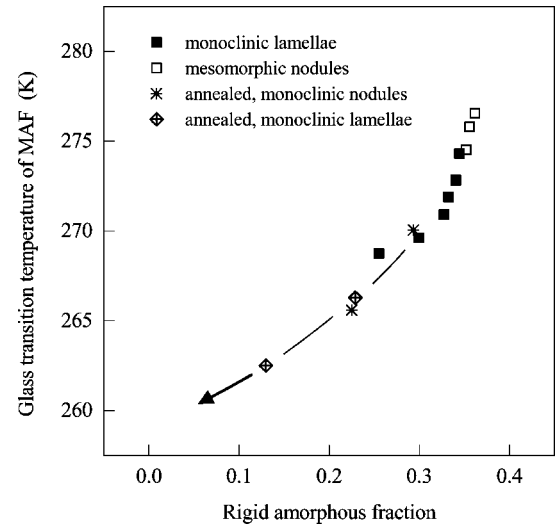

Figure 8. Glass transition temperature of iPP as a function of the rigid amorphous fraction. The filled and open squares represent data which were obtained on non-annealed samples containing lamellae or nodules, respectively, and the cross-filled tilted squares and asterisks represent data which were obtained on annealed samples. Glass transition temperatures were obtained by DSC.

6b, is not complete and that we also found few literature data, which showed no clear correlation between the RAF/MAF ratio and the crystallinity.[24,59] A straightforward conclusion from the data of Figure 6b is a low degree of coupling of the crystalline and amorphous phases and therefore a relatively high mobility of the amorphous phase in samples of high crystallinity. As a general trend, crystallization at low supercooling or at a low rate of cooling allows formation of thick crystals with basal planes of low free energy, since kinetic restrictions of the crystallization process are minimal. This, in turn, is connected to reduced covalent linkage between the crystalline and amorphous phases. Formation of layers of higher defect concentration at the lateral surfaces of primary grown perfect crystals, or formation of defective and thinner crystals as a result of secondary crystallization, may only be expected in the final stage of the crystallization process, increasing the RAF.[60,61]

4.2. Effect of the Crystal Habit on the RAF. The RAF data of Figure 5 do not allow identification of an influence of the crystal shape on the RAF. In other words, samples of identical crystallinities, independent of whether they contain nodules or lamellae, exhibit similar RAFs if the structures and therefore the surface free energies of the basal planes are identical. Generation of identical surface structures of nodules and lamellae was achieved by annealing at elevated temperature and was evidenced by subsequent thermal analysis of the temperature of melting. Annealed samples, regardless of whether they contain lamellae or nodules, exhibit identical temperatures of melting, which points, according to the Gibbs−Thomson equation, to the presence of crystals of identical thermodynamic stabilities.[41] Though it is expected that the lateral surfaces of the crystals are not considered as a major source for immobilization of the amorphous phase, to the best of our knowledge, experimental evidence has not yet been provided in the literature. In fact, the data of the present study suggest that the lateral surfaces of crystals do not contribute to formation of the RAF. Figure 7 shows equiaxed nodules with a volume of $1 \times 1 \times 1$ au^3 (left) and a lamella with a volume of $5 \times 4 \times 1$ au^3 (right). The only difference between the nodules and the lamella are the lateral dimensions. Identical volumes of 20 au^3, i.e., identical crystallinities, and identical areas of the basal planes are achieved if 20 nodules are present. The total area of the lateral surfaces of the nodules in this particular scenario, however, would be more than 4× the area of the lateral surfaces of the lamellae. If the lateral surfaces of the crystals significantly contribute to an immobilization of the amorphous phase, then samples with nodular crystals need to show a considerably larger RAF than samples which contain lamellae. This, however, is not observed and confirms the assignment of the RAF to the basal planes of the crystals.

Note that we do not intend to enter a quantitative discussion of this topic. This would require extremely accurate data about the crystal thickness, which is a prerequisite for an exact calculation of the ratio of the areas of the lateral surfaces and of the basal planes. Albeit the AFM images of Figure 1 can advantageously be used for a qualitative characterization of the crystal morphology, and for monitoring relative changes of the dimensions on annealing, we hesitate to extract quantitative information about the absolute thickness of the crystals, mainly due to errors originating from the geometry of the AFM tip.[38] Additional errors in image analysis, despite not being evidenced yet, may be caused by the existence of the RAF itself. The mechanical characteristics of the RAF in the glassy state may be similar to the mechanical characteristics of the crystalline phase; i.e., AFM analysis using the non-contact intermittent mode may overestimate the crystalline fraction/crystal dimensions. Nonetheless, the above-described concerns do not affect the major conclusion of relating the RAF to the basal planes of the crystals and not to their lateral faces.

4.3. Mobility of the MAF. The data of Figure 3 reveal a strong influence of the history of crystallization on the glass transition temperature of the MAF. An increase of the cooling rate on primary melt crystallization from 10^{-1} to 10^2-10^3 K s^{-1} is connected with a distinct increase of the glass transition temperature by more than 10−20 K. Subsequent annealing, in turn, leads to a decrease of the glass transition temperature, with the largest changes obtained in samples which initially were rapidly crystallized. In Figure 4, glass transition temperature data were plotted as a function of the enthalpy-based crystallinity, showing lower values in preparations of high crystallinity. This observation is paralleled by detection of a low amount of the RAF in samples of relatively high crystallinity. We assume therefore that the glass transition temperature of the MAF may be controlled by the mobility and the amount of the RAF. To confirm this assumption, we plotted the glass transition temperature of the MAF as a function of the RAF in Figure 8. The data, unambiguously, reveal that an increasing RAF is connected with an increase of the glass transition temperature. We consider this correlation as evidence for a distinct coupling of the MAF

and RAF. The mobility of the MAF, as expressed by its glass transition temperature, decreases if a large amount of RAF is evident due to the presence of crystals with a rather imperfect structure of the basal planes. This coupling, however, does not affect the observation of two distinct fractions of the amorphous phase; i.e., we did not detect a continuous increase of the mobility of the amorphous phase as a function of the distance from the crystal surface by thermal analysis of the glass transition.

Finally, the data of Figure 8 prove high reliability/accuracy of the experiments performed in this study. Experimental raw data include the glass transition temperature of the MAF and the amount of RAF. Extrapolation of the glass transition temperature of the MAF to zero RAF yields a value of 258−259 K. This value is within the range of glass transition temperatures reported for fully amorphous PP.[30−34]

Acknowledgment. This research was supported by funding from the Ministry of Culture of Saxony-Anhalt (Germany), by an STSM grant within the EU COST-P12 program for Q.Z., and by a grant from the EU SOKRATES/ERASMUS program for D.M.

References and Notes

(1) Strobl, G. *The Physics of Polymers*; Springer: Berlin, 2007.
(2) Wunderlich, B. *Macromolecular Physics, Vol. 1, Crystal Structure, Morphology, Defects*; Academic Press: New York, 1973.
(3) Androsch, R.; Wunderlich, B. Scanning calorimetry. In *Macromolecular Engineering: Precise Synthesis, Materials Properties, Applications, Vol. 3, Structure-Property Correlation and Characterization Techniques*; Matyjaszewski, K., Gnanou, Y., Leibler, L., Eds.; Wiley-VCH: Weinheim, Germany, 2007.
(4) Ishida, Y.; Yamafuji, K.; Ito, H.; Takayanagi, M. *Kolloid Z. Z. Polym.* **1962**, *14*, 97.
(5) Groeninckx, G.; Berghmans, H.; Smets, G. *J. Polym. Sci., Polym. Phys. Ed.* **1976**, *14*, 591.
(6) Wissler, G. E.; Crist, B., Jr *J. Polym. Sci., Polym. Phys. Ed.* **1980**, *18*, 1257.
(7) Suzuki, H.; Grebowicz, J.; Wunderlich, B. *Br. Polym. J.* **1985**, *17*, 1.
(8) Kitamaru, R.; Horii, F.; Murayama, K. *Macromolecules* **1986**, *19*, 636.
(9) Kolesov, I. S.; Androsch, R.; Radusch, H.-J. *Macromolecules* **2005**, *38*, 445.
(10) Grebowicz, J.; Lau, S. F.; Wunderlich, B. *J. Polym. Sci., Polym. Symp.* **1984**, *71*, 19.
(11) Schick, C.; Wurm, A.; Mohamed, A. *Thermochim. Acta* **2002**, *392/393*, 303.
(12) Di Lorenzo, M. L.; Righetti, M. C. *Polymer* **2008**, *49*, 1323.
(13) Chen, H.; Cebe, P. *J. Therm. Anal. Calorim.* **2007**, *89*, 4.
(14) Menczel, J.; Wunderlich, B. *J. Polym. Sci., Polym. Lett. Ed.* **1981**, *19*, 261.
(15) (a) Schick, C.; Krämer, L.; Mischok, W. *Acta Polym.* **1985**, *36*, 47. (b) Schick, C.; Fabry, F.; Schnell, U.; Stoll, G.; Deutschbein, L.; Mischok, W. *Acta Polym.* **1988**, *39*, 705. (c) Schick, C.; Wigger, J.; Mischok, W. *Acta Polym.* **1990**, *41*, 137.
(16) Cheng, S. Z. D.; Pan, R.; Wunderlich, B. *Makromol. Chem.* **1988**, *189*, 2443.
(17) Pyda, M.; Nowak-Pyda, E.; Mays, J.; Wunderlich, B. *J. Polym. Sci., Part B: Polym. Phys.* **2004**, *42*, 4401.
(18) Schick, C.; Wurm, A.; Merzlyakov, M.; Minakov, A.; Marand, H. *J. Therm. Anal. Calorim.* **2001**, *64*, 549.
(19) Wunderlich, B. *Prog. Polym. Sci.* **2003**, *28*, 383.
(20) Sargsyan, A.; Tonoyan, A.; Davtyan, S.; Schick, C. *Eur. Polym. J.* **2007**, *43*, 3113.
(21) Androsch, R. *Eur. Polym. J.* **2007**, *43*, 93.
(22) Sauer, B. B.; Hsiao, B. *Polymer* **1995**, *36*, 2553.
(23) Olson, B. G.; Lin, J.; Nazarenko, S.; Jamieson, A. M. *Macromolecules* **2003**, *36*, 7618.
(24) Rastogi, R.; Vellinga, W. P.; Rastogi, S.; Schick, C.; Meijer, H. E. H. *J. Polym. Sci., Part B: Polym. Phys.* **2004**, *42*, 2092.
(25) Androsch, R.; Wunderlich, B. *Polymer* **2005**, *46*, 12556.
(26) Fu, Y.; Annis, B.; Boller, A.; Jin, Y.; Wunderlich, B. *J. Polym. Sci., Part B: Polym. Phys.* **1994**, *42*, 2289.
(27) Varma-Nair, M.; Agarwal, P. K. *Polym. Mater. Sci. Eng.* **1999**, *81*, 310.
(28) Hedesiu, C.; Demco, D. E.; Kleppinger, R.; Vanden Poel, G.; Gijsbers, W.; Blümich, B.; Remerie, K.; Litvinov, V. M. *Macromolecules* **2007**, *40*, 3977.
(29) Agarwal, M. K.; Schultz, J. M. *Polym. Eng. Sci.* **1981**, *21*, 776.
(30) Hsu, C. C.; Geil, P. H.; Miyaji, H.; Asai, K. *J. Polym. Sci., Polym. Phys. Ed.* **1986**, *24*, 2379.
(31) Caldas, V.; Brown, G. R.; Nohr, R. S.; MacDonald, J. G.; Raboin, L. E. *Polymer* **1994**, *35*, 899.
(32) Ogawa, T.; Miyaji, H.; Asai, K. *J. Phys. Soc. Jpn.* **1985**, *54*, 3668.
(33) Miyamoto, Y.; Fukao, K.; Yoshida, T.; Tsurutani, N.; Miyaji, H. *J. Phys. Soc. Jpn.* **2000**, *69*, 1735.
(34) Andersson, S. P.; Andersson, O. *Int. J. Thermophys.* **1997**, *18*, 845.
(35) De Santis, F.; Adamovsky, S.; Titomanlio, G.; Schick, C. *Macromolecules* **2006**, *39*, 2562.
(36) Gradys, A.; Sajkiewicz, P.; Minakov, A. A.; Adamovsky, S.; Schick, C.; Hashimoto, T.; Saijo, K. *Mater. Sci. Eng.* **2005**, *A413−414*, 442.
(37) Brucato, V.; Piccarolo, S.; La Carruba, V. *Chem. Eng. Sci.* **2002**, *57*, 4129.
(38) Zia, Q.; Androsch, R.; Radusch, H.-J.; Ingolič, E. *Polym. Bull.* **2008**, *60*, 791.
(39) Zia, Q.; Androsch, R.; Radusch, H.-J.; Piccarolo, S. *Polymer* **2006**, *47*, 8163.
(40) Androsch, R. *Macromolecules* **2008**, *41*, 833.
(41) Zia, Q.; Radusch, H.-J.; Androsch, R. *Polymer* **2007**, *48*, 3504.
(42) Wunderlich, B. *Thermal Analysis of Polymeric Materials*; Springer: Berlin, 2005.
(43) Mathot, V. B. F.; Pijpers, M. F. J. *Thermochim. Acta* **1989**, *151*, 241.
(44) Wunderlich, B. *Pure Appl. Chem.* **1995**, *67*, 1019.
(45) Peterlin, A. *Makromol. Chem.* **1964**, *74*, 107.
(46) Hikosaka, M. *Polymer* **1987**, *28*, 1257; **1990**, *31*, 458.
(47) Farrow, G. *Polymer* **1963**, *4*, 191.
(48) Grubb, D. T.; Yoon, D. Y. *Polym. Commun.* **1986**, *27*, 84.
(49) Gezovich, D. M.; Geil, P. H. *Polym. Eng. Sci.* **1968**, *8*, 202.
(50) Piccarolo, S. *J. Macromol. Sci., Phys.* **1992**, *B31*, 501.
(51) Fichera, A.; Zannetti, R. *Makromol. Chem.* **1975**, *176*, 1885.
(52) Zannetti, R.; Celotti, G.; Fichera, A.; Francesconi, R. *Makromol. Chem.* **1969**, *128*, 137.
(53) O'Kane, W. J.; Young, R. J.; Ryan, A. J.; Bras, W.; Derbyshire, G. E.; Mant, G. R. *Polymer* **1994**, *35*, 1352.
(54) Jin, Y.; Hiltner, A.; Baer, E.; Masirek, R.; Piorkowska, E.; Galeski, A. *J. Polym. Sci., Part B: Polym. Phys.* **2006**, *44*, 1795.
(55) Duncan, J. C.; van de Velde, J. G.; Wetton, R. E. *Kautsch. Gummi Kunstst.* **1991**, *44*, 768.
(56) Donth, E. *The Glass Transition, Relaxation Dynamics in Liquids and Disordered Materials*; Springer Series in Materials Science, Vol. *48*, Springer: New York, 2001.
(57) Alvarez, C.; Šics, I.; Nogales, A.; Denchev, Z.; Funari, S. S.; Ezquerra, T. A. *Polymer* **2004**, *45*, 3959.
(58) Huo, P.; Cebe, P. *J. Polym. Sci., Part B: Polym. Phys.* **1992**, *30*, 239.
(59) Okazaki, I.; Wunderlich, B. *J. Polym. Sci., Part B: Polym. Phys.* **1996**, *34*, 2941.
(60) Wang, Z.-G.; Hsiao, B. S.; Sauer, B. B.; Kampert, W. G. *Polymer* **1999**, *40*, 4615.
(61) Righetti, M. C.; Tombari, E.; Angiuli, M.; Di Lorenzo, M. L. *Thermochim. Acta* **2007**, *462*, 15.

MA801455M